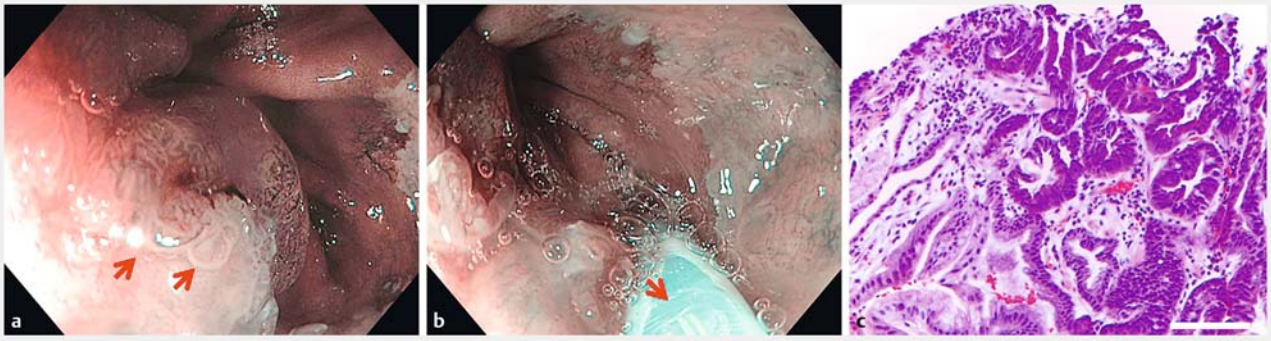

▶ **Fig. e1** Optical coherence tomography (OCT) acquisition with correlated biopsy/endoscopic mucosal resection (EMR) histology. **a** White-light endoscopy (WLE)/narrow-band imaging (NBI) showing dysplastic lesion (arrows) at the squamocolumnar junction. **b** WLE/NBI with OCT catheter (arrow) introduced through a dual-channel endoscope to enable biopsy/EMR from the subsequent OCT-imaged region. **c** Hematoxylin and eosin histology of resected specimen indicating high grade dysplasia. Scale bar 100 µm.

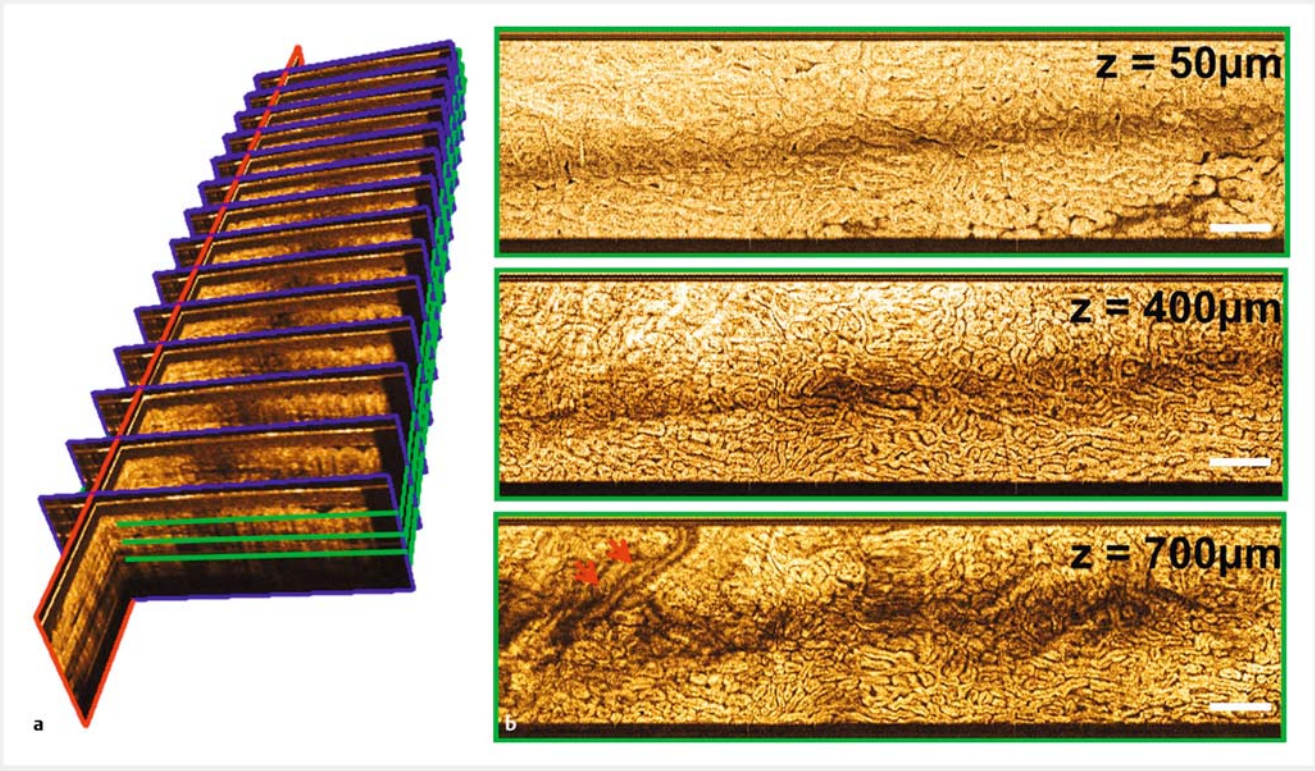

▶ **Fig. e2** Volumetric optical coherence tomography (OCT) dataset visualization. **a** Representation of volumetric OCT dataset showing cross-sectional (blue frame), longitudinal (red frame), and en face views (green frame), which are intrinsically co-registered. The series of cross-sectional OCT images at sequential longitudinal positions could be scrolled for rapid viewing, or specific cross-sections from en face regions of interest could be viewed selectively. **b** Depth-resolved en face OCT images at various depths. The en face OCT image near the surface shows the superficial mucosal architecture, whereas deeper images delineate the mucosal patterns in greater detail and contrast. At depths near the muscularis mucosa/submucosa (~ 700 µm) boundary, vascular features can be observed. Scattering from blood produces attenuation of OCT signals in deeper levels; arrows point to a shadow produced by a large vessel. En face OCT images in this figure are cropped from a larger dataset to exclude regions that are out of contact with the OCT catheter. Scale bars 1 mm.

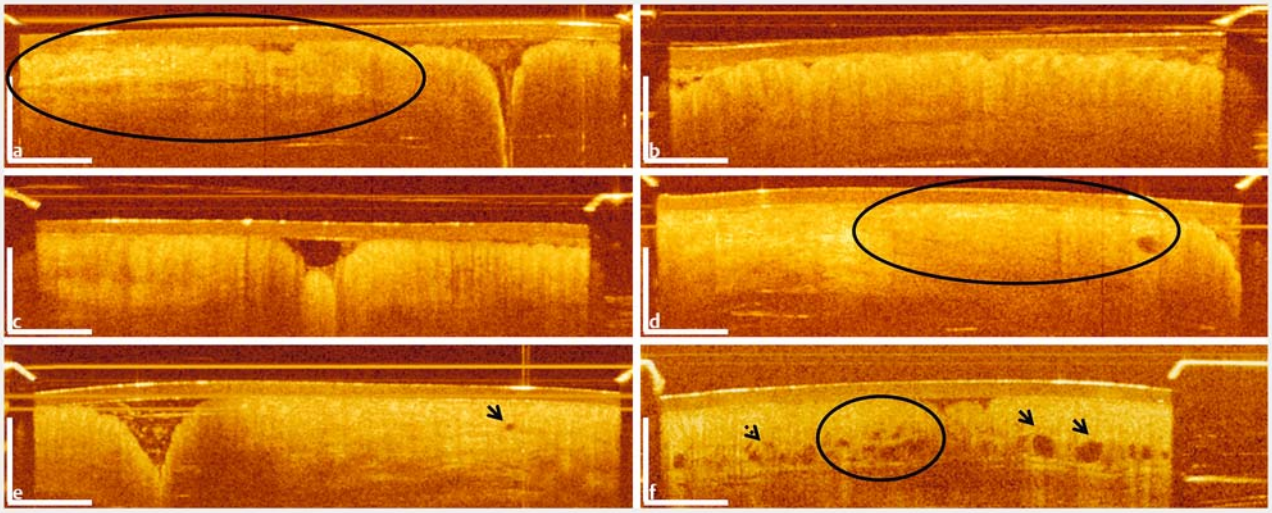

▶ **Fig. e4** Cross-sectional optical coherence tomography (OCT) features assessed include mucosal layering, surface signal vs. subsurface, and atypical glands. **a-b** Representative cross-sectional OCT images showing presence or absence of mucosal layering, respectively. The oval indicates an area with mucosal layering present. **c-d** Representative cross-sectional OCT images showing surface signal ≤ subsurface, and surface signal > subsurface, respectively. The oval indicates an area with surface signal > subsurface. **e** Representative cross-sectional OCT image showing normal-appearing glandular architecture. Solid arrow points to a dilated gland with normal appearance. **f** Representative cross-sectional OCT image showing atypical glandular architecture. Solid arrows point to atypical glands with irregular size and shape. Dashed arrow points to an atypical debris-filled gland. The oval marks an area with clustered atypical glands. Scale bars 1 mm.

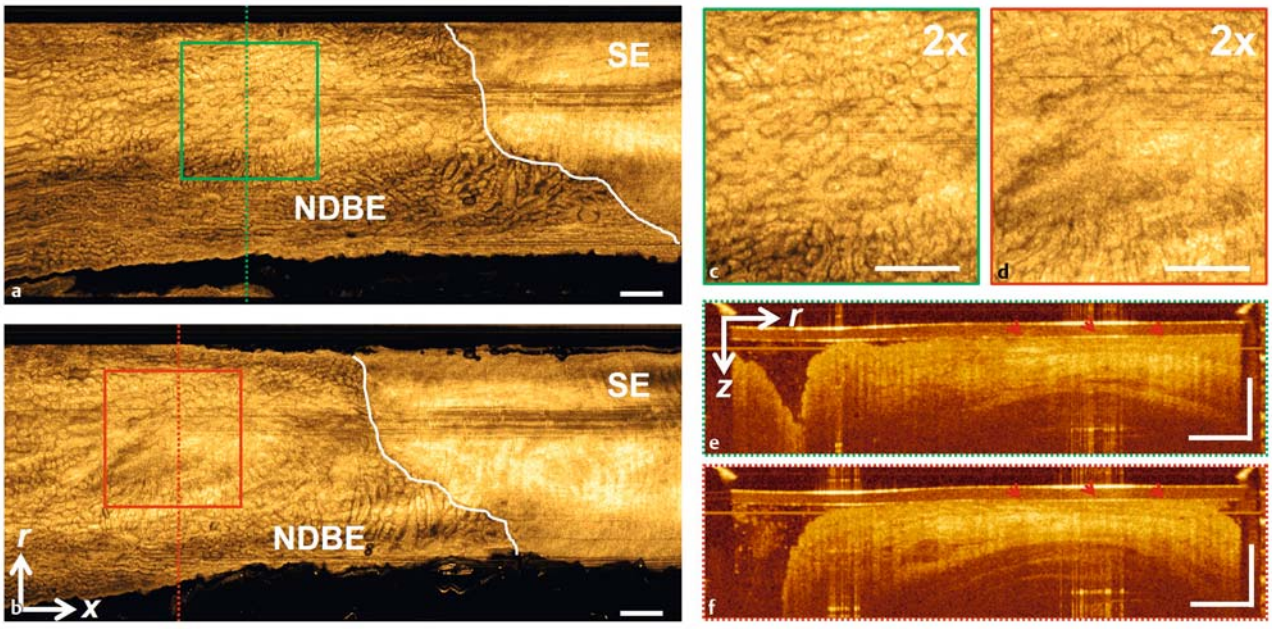

▶ **Fig. e6** Effects of catheter pressure on tissue. Nondysplastic Barrett's esophagus (NDBE) datasets acquired approximately at the same longitudinal position along the esophagus with different catheter pressure. **a** En face optical coherence tomography (OCT) at ~ 400 µm below the tissue surface showing squamocolumnar junction, demarcated by the white line, and regular mucosal patterns in the NDBE region. **b** En face OCT at ~ 400 µm below the tissue surface with a higher catheter pressure. Distortion of the regular mucosal patterns is apparent. **c–d** × 2 zoom over the boxed areas in **a** and **b**, respectively, showing the region where catheter pressure produces the largest distortion of mucosal patterns. **e-f** Cross-sectional OCT images at the dotted lines in **a** and **b**, respectively, showing artifactually decreased mucosal layer thickness (arrows), and increased submucosal layer signal due to pressure. r, circumferential direction; x, longitudinal direction; z, depth direction; SE, normal squamous epithelium. Scale bars 1 mm.

▶ **Table e1** Comparison of ultrahigh-speed endoscopic optical coherence tomography with volumetric laser endomicroscopy, magnification narrow-band imaging, and probe-based confocal laser endomicroscopy.

	Ultrahigh-speed OCT with micromotor catheters	VLE[1]	Magnification NBI (GIF Q240Z/260Z series)[2]	pCLE[3,4]
Field of view (single acquisition/image)	~ 10 mm × 16 mm[5]	~ 60 mm × 60 mm	~ 3 mm diameter circle at maximal magnification	240 – 600 µm diameter circle
Imaging time (single acquisition/image)	8 seconds	90 seconds	~ 30 msec (video rate)	~ 80 msec (12 images per second)
Frame sampling interval	5 µm	~ 50 µm	N/A	N/A
Depth (axial) scan rate	600 000 A-scans/sec	50 000 A-scans/sec	N/A	N/A
Lateral resolution	20 µm	40 µm	6 – 8 µm	1 – 4 µm
Depth (axial) resolution	8 µm	7 µm	Low, see discussion in **Appendix e6**	5 µm
Depth (axial) range (imaging depth)	2.4 mm	3 mm	Shallow, see discussion in **Appendix e6**	40 – 130 µm
Catheter diameter	3.4 mm	14 mm, 17 mm, 20 mm balloon	10 mm (endoscope)	2.5 mm
Main strengths	High imaging speed reduces motion artifacts Depth-resolved en face visualization of mucosal patterns	Large area imaging Recent systems have laser marking for more precise histological correlation	NBI integrated with endoscope Visualizes mucosal and vascular patterns	Cellular details visible
Main limitations	Limited circumferential coverage	Slow imaging speed limits en face visualization	Depth-resolved imaging is not possible	Small field of view Requires contrast agents

N/A, not applicable; NBI, narrow-band imaging; OCT, optical coherence tomography; pCLE, probe-based confocal laser endomicroscopy; VLE, volumetric laser endomicroscopy.
[1] Swager AF et al. Gastrointest Endosc 2017; 85: 918 – 926.e7 [ref. 6 in Supplement].
[2] Yao K. Zoom gastroscopy: magnifying endoscopy in the stomach: Springer Japan; 2013 [ref. 18 in Supplement].
[3] Canto MI. Gastroenterol Clin North Am 2010; 39: 759 – 769 [ref. 19 in Supplement].
[4] Endoscope-based CLE was not included because it has been discontinued.
[5] The longitudinal pullback length used in this study was standardized to 16 mm, but can be increased.

▶ **Table e2** Association of en face and cross-sectional optical coherence tomography features with correlated histological diagnosis stratified into nondysplastic Barrett's esophagus, low grade dysplasia, and high grade dysplasia/esophageal adenocarcinoma.

	NDBE*, n/N (%)	LGD*, n/N (%)	HGD/EAC*, n/N (%)
Proportion of irregular mucosal patterns	39/111 (35)	18/18 (100)	33/33 (100)
Proportion of atypical glands (> 5)	66/111 (59)	15/18 (83)	23/33 (70)
▪ Proportion of atypical glands under irregular mucosal patterns	33/111 (30)	15/18 (83)	23/33 (70)
Proportion of absent mucosal layering	55/111 (50)	9/18 (50)	9/33 (27)
Proportion of surface signal > subsurface	33/111 (30)	5/18 (28)	10/33 (30)

EAC, esophageal adenocarcinoma; HGD, high grade dysplasia; LGD, low grade dysplasia; NDBE, nondysplastic Barrett's esophagus.
* Overall for three readers.

▶ **Table e3** Histology of the optical coherence tomography datasets.

OCT datasets with correlated biopsy/EMR histology, n	NDBE	LGD	HGD	EAC	Total
Training session	8	3	2	0	13
Pretest session	4	1	2	0	7
Validation session	37	6	9	2	54

EAC, esophageal adenocarcinoma; EMR, endoscopic mucosal resection; HGD, high grade dysplasia; LGD, low grade dysplasia; NDBE, nondysplastic Barrett's esophagus; OCT, optical coherence tomography.

▶ **Table e4** Patient demographics and characteristics of optical coherence tomography datasets with correlated biopsy/endoscopic mucosal resection histology.

Patient demographics (n = 44)	
▪ Age, mean (SD), years	70 (7.6)
▪ Sex, male, n (%)	43 (98)
▪ Race, white, n (%)	43 (98)
Baseline histology, n (%)	
▪ NDBE	30 (68)
▪ Neoplasia, LGD/HGD/EAC	8/5/1 (32)
▪ Previously treated	4 (9)
▪ Treatment naïve	10 (23)
Length of BE, mean (SD), cm	
▪ Circumferential extent (C)	2.3 (3.9)
▪ Maximum extent (M)	3.9 (4.1)
Number of OCT datasets with correlated biopsy/EMR histology per subject, median (range)	1 (1 – 5)
Characteristics of OCT datasets with correlated biopsy/EMR histology (n = 74), n (%)	
▪ NDBE	49 (66)
▪ From previously treated patients	0 (0)
▪ From treatment-naïve patients	49 (66)
▪ Neoplasia, LGD/HGD/EAC, n (%)	10/13/2 (34)
▪ From previously treated patients	13 (18)
▪ From treatment-naïve patients	12 (16)

BE, Barrett's esophagus; EAC, esophageal adenocarcinoma; EMR, endoscopic mucosal resection; HGD, high grade dysplasia; LGD, low grade dysplasia; NDBE, non-dysplastic Barrett's esophagus; OCT, optical coherence tomography.

▶ **Table e5** Association of irregular mucosal patterns and atypical glands with correlated histological diagnosis and treatment history.

	Reader 1, n/N	Reader 2, n/N	Reader 3, n/N	Overall, n/N (%)	*P* value[1]
Proportion of irregular mucosal patterns					
In NDBE	13/37	11/37	15/37	39/111 (35)	<0.001[2,3]
▪ Short-segment (≤ 3 cm) NDBE	8/17	7/17	7/17	22/51 (43)	0.11[4], 0.43[5]
▪ Long-segment (> 3 cm) NDBE	5/20	4/20	8/20	17/60 (28)	
▪ Away (> 3 cm) from GEJ	4/12	2/12	3/12	9/36 (25)	0.49[6]
▪ Near (≤ 3 cm) the GEJ	1/8	2/8	5/8	8/24 (33)	
In neoplasia	17/17	17/17	17/17	51/51 (100)	
▪ Treatment naïve	8/8	8/8	8/8	24/24 (100)	>0.99[7]
▪ Previously treated	9/9	9/9	9/9	27/27 (100)	
Proportion of atypical glands (> 5)					
In NDBE	23/37	20/37	23/37	66/111 (59)	0.07[2], <0.001[3]
▪ Short-segment (≤ 3 cm) NDBE	14/17	14/17	12/17	40/51 (78)	<0.001[4], 0.28[5]
▪ Long-segment (> 3 cm) NDBE	9/20	6/20	11/20	26/60 (43)	
▪ Away (> 3 cm) from GEJ	3/12	2/12	5/12	10/36 (28)	0.003[5]
▪ Near (≤ 3 cm) the GEJ	6/8	4/8	6/8	16/24 (67)	
In neoplasia	11/17	13/17	14/17	38/51 (75)	
▪ Treatment naïve	7/8	8/8	8/8	23/24 (96)	0.001[6]
▪ Previously treated	4/9	5/9	6/9	15/27 (56)	

GEJ, gastroesophageal junction; NDBE, nondysplastic Barrett's esophagus.
[1] Analyses conducted separately for the two groups (proportion of irregular mucosal patterns and proportion of atypical glands [> 5]).
[2] vs. in neoplasia.
[3] vs. treatment-naïve patients with neoplasia.
[4] vs. long-segment NDBE.
[5] vs. near the GEJ.
[6] vs. near the GEJ.
[7] vs. previously treated patients.

▶ **Table e6** Association of absent mucosal layering and surface signal > subsurface with correlated histological diagnosis and treatment history.

	Reader 1, n/N	Reader 2, n/N	Reader 3, n/N	Overall, n/N (%)	*P* value[1]
Proportion of absent mucosal layering					
In NDBE	23/37	13/37	19/37	55/111 (50)	0.09[2], 0.01[3]
In neoplasia	8/17	6/17	4/17	18/51 (35)	
▪ Treatment naïve	3/8	2/8	0/8	5/24 (21)	
▪ Previouslytreated	5/9	4/9	4/9	13/27 (48)	
Proportion of surface signal > subsurface					
In NDBE	15/37	7/37	11/37	33/111 (30)	0.97[2], 0.38[3]
In neoplasia	5/17	6/17	4/17	15/51 (29)	
▪ Treatment naïve	1/8	3/8	1/8	5/24 (21)	
▪ Previously treated	4/9	3/9	3/9	10/27 (37)	

NDBE, nondysplastic Barrett's esophagus.
[1] Analyses conducted separately for the two groups (Proportion of absent mucosal layering and Proportion of surface signal > subsurface).
[2] vs. in neoplasia.
[3] vs. treatment-naïve patients with neoplasia.

▶ **Table e8** Interobserver agreement of en face and cross-sectional optical coherence tomography features.

	Kappa value (95 %CI)
Irregular mucosal patterns	0.73 (0.69 – 0.77)
VLE-DA features of	
▪ Absent mucosal layering	0.6 (0.56 – 0.64)
▪ Surface signal > subsurface	0.17 (0.13 – 0.21)
▪ Atypical glands	0.73 (0.69 – 0.77)

CI, confidence interval; VLE-DA, volumetric laser endomicroscopy diagnostic algorithm.

▶ **Table e9** Average reading times per dataset.

	Reader 1	Reader 2	Reader 3	Overall
En face assessment, mean (SD), seconds	53 (48)	80 (66)	47 (22)	60* (51)
Cross-sectional assessment, mean (SD), seconds	69 (40)	71 (56)	66 (36)	69* (42)
Overall assessment, mean (SD), seconds	122 (70)	152 (93)	113 (35)	129 (72)

* *P* value for the comparison between the average en face and cross-sectional assessment is 0.12.

▶ **Table e10** Association of mucosal patterns with absent mucosal layering and surface signal > subsurface, stratified according to correlated histological diagnosis.

	Reader 1, n/N	Reader 2, n/N	Reader 3, n/N	Overall, n/N (%)	*P* value[1]
Proportion of absent mucosal layering					
Under regular mucosal patterns	16/54	11/54	11/54	38/162 (24)	0.7[2]
▪ In NDBE	16/37	11/37	11/37	38/111 (34)	< 0.001[3]
▪ In neoplasia	0/17	0/17	0/17	0/51 (0)	
Under irregular mucosal patterns	15/54	8/54	12/54	35/162 (22)	
▪ In NDBE	7/37	2/37	8/37	17/111 (15)	0.004[4]
▪ In neoplasia	8/17	6/17	4/17	18/51 (35)	
Proportion of surface signal > subsurface					
Under regular mucosal patterns	11/54	5/54	9/54	25/162 (15)	0.76[2]
▪ In NDBE	11/37	5/37	9/37	25/111 (23)	< 0.001[3]
▪ In neoplasia	0/17	0/17	0/17	0/51 (0)	
Under irregular mucosal patterns	9/54	8/54	6/54	23/162 (14)	
▪ In NDBE	4/37	2/37	2/37	8/111 (7)	< 0.001[4]
▪ In neoplasia	5/17	6/17	4/17	15/51 (29)	

NDBE, nondysplastic Barrett's esophagus.
[1] Analyses conducted separately for the two groups (proportion of absent mucosal layering and proportion of surface signal > subsurface).
[2] vs. under irregular mucosal patterns.
[3] vs. under regular mucosal patterns in neoplasia.
[4] vs. under irregular mucosal patterns in neoplasia.

▶ **Table e11** Association of en face optical coherence tomography and criteria of volumetric laser endomicroscopy diagnostic algorithm with correlated histological diagnosis and treatment history.

	Reader 1, n/N	Reader 2, n/N	Reader 3, n/N	Overall, n/N (%)	*P* value
Proportion of irregular mucosal patterns on en face OCT with VLE-DA features of dysplasia on cross-sectional OCT					
In NDBE	8/37	9/37	8/37	25/111 (23)	<0.001*
In neoplasia	13/17	14/17	12/17	39/51 (77)	
▪ Treatment naïve	6/8	8/8	8/8	22/24 (92)	
▪ Previously treated	7/9	6/9	4/9	17/27 (63)	

NDBE, nondysplastic Barrett's esophagus; OCT, optical coherence tomography; VLE-DA, volumetric laser endomicroscopy diagnostic algorithm.
* vs. in neoplasia and vs. in treatment-naïve patients with neoplasia.

▶ **Table e12** Confidence of the readers' assessment of en face and cross-sectional optical coherence tomography features.

	Reader 1, n/N	Reader 2, n/N	Reader 3, n/N	Overall, n/N (%)
Irregular mucosal patterns				
High confidence	47/54	43/54	50/54	140/162 (86)
NDBE	30/37	30/37	34/37	94/111 (85)
Neoplasia	17/17	13/17	16/17	46/51 (90)
All features[1]				
High confidence	41/54	41/54	49/54	131/162 (81)
NDBE	28/37	30/37	34/37	92/111 (83)
Neoplasia	13/17	11/17	15/17	39/51 (77)

NDBE, nondysplastic Barrett's esophagus.
[1] En face optical coherence tomography (OCT) feature of irregular mucosal patterns and all three cross-sectional OCT features were assessed with high confidence.

Appendix e1 Technical details of the ultrahigh-speed endoscopic OCT instrument

The prototype ultrahigh-speed endoscopic OCT instrument [1] used in this study operated at 600 000 depth (axial) scans/second, >10 times faster than commercial instruments [2]. Distal rotary beam scanning was performed using a 3.4 mm outer diameter (OD) OCT micromotor catheter with an internal 2.0 mm OD micromotor (Namiki, Japan) at 400 Hz (400 cross-sectional OCT images per second). The internal assembly of the catheter was proximally pulled back at 2 mm/second to generate volumetric datasets (**Fig. e2**). Each OCT volume was acquired in 8 seconds over a ~10 mm × 16 mm (circumferential × longitudinal) area with 3200 cross-sectional OCT images of 1500 A-scans each. The depth (axial) range was 2.4 mm with an 8 µm (full width half maximum) resolution and 20 µm lateral image resolution. Cross-sectional OCT images were corrected for nonuniform rotational distortion to improve en face visualization [3]. En face OCT data at a given depth were viewed by summing over +/–50 µm depth (100 µm projection range) to improve contrast and reduce noise. **Table e1** compares the prototype OCT instrument with VLE, magnification NBI, and pCLE.

Appendix e2 Supplemental discussion on subgroup analysis of LGD

In this study, LGD datasets were grouped with HGD and EAC datasets, and all were categorized as neoplasia. This contrasts with some previous studies that either excluded LGD or grouped it with NDBE. The association of en face and cross-sectional OCT features with correlated histological diagnosis when the neoplasia datasets are separated into LGD vs. HGD/EAC is shown in **Table e2**. Irregular mucosal patterns were present in 35% of NDBE datasets, in 100% of LGD datasets, and in 100% of HGD/EAC datasets. Atypical glands were present in 59% of NDBE datasets, in 83% of LGD datasets, and in 70% of HGD/EAC datasets. Atypical glands under irregular mucosal patterns were present in 30% of NDBE datasets, in 83% of LGD datasets, and in 70% of HGD/EAC datasets. Mucosal layering was absent in 50% of NDBE datasets, in 50% of LGD datasets, and in 27% of HGD/EAC datasets. Surface signal>subsurface occurred in 30% of NDBE datasets, in 28% of LGD datasets, and in 30% of HGD/EAC datasets. These findings suggest that LGD exhibited irregular mucosal patterns and atypical glands features that are more similar to HGD/EAC than to NDBE. Our results are consistent with recent reports suggesting that endoscopic treatment is indicated for LGD [4]. The histological diagnosis of all LGD cases was made by a specialized expert gastrointestinal (GI) pathologist with >15 years of experience in GI pathology (Q.H.). Third-party confirmation from expert referral centers, such as The Joint Pathology Center, MD, or the Brigham and Women’s Hospital, MA, was obtained when necessary.

Appendix e3 Definitions and discussion of cross-sectional OCT features and VLE-DA

Mucosal layering in cross-sectional OCT was defined as absent (complete effacement) if layering was absent in >50% of the images in the series, otherwise it was defined as present (partial effacement, **Fig. e4**). Surface signal was defined as higher than subsurface signal (surface signal>subsurface) if it was higher in >50% of the images in the series, otherwise it was defined as lower or equal (surface signal≤subsurface). Atypical glands were defined to be present if there was a total of >5 atypical glands in the image series. Dilated glands were considered atypical glands if they had irregular size, shape, contained internal debris, or had clustered appearance, as in previous descriptions [5,6]. These features were combined using VLE-DA to assess cross-sectional OCT [5]: datasets with mucosal layering present and ≤5 atypical glands, or datasets with mucosal layering absent and surface signal≤subsurface were classified as VLE-DA negative for neoplasia; whereas datasets with mucosal layering present and >5 atypical glands, or datasets with mucosal layering absent and surface signal>subsurface were classified as VLE-DA positive for neoplasia.

In this study, we also used VLE-DA to assess cross-sectional OCT images because it is one of few validated protocols for an image series, rather than individual images. Although it has not yet been tested in vivo, its performance was reported to be better than previous OCT dysplasia detection criteria [7]. Readers assessed each cross-sectional OCT feature independently, so that separate cross-sectional OCT features could be tested in addition to VLE-DA, which uses cross-sectional features in an algorithm.

As indicated in the reading workflow in **Appendix e4**, cross-sectional OCT features were assessed immediately after en face OCT reading without a separate reading

session or washout period. Our reading protocol was designed to investigate volumetric OCT reading, where the en face and cross-sectional (orthoplane) information are used jointly. However, this may result in a bias in the cross-sectional OCT reading.

Appendix e4 Training and volumetric OCT reading workflow

Reader 1 was a nonclinician OCT trainee, reader 2 was an attending gastroenterologist with OCT experience, and reader 3 was a clinical GI trainee with no prior OCT experience. In a pretest following the training, readers identified features independently, but subsequently received feedback from the investigator. Readers were required to assess >75% of the features in accord with the study investigator's assessment to participate in the validation reading.

Readings were performed using open source software (3D Slicer [8]) that allowed simultaneous orthoplane visualization of the en face and cross-sectional OCT image series with brightness and contrast adjustment. During training, pretest, and validation readings, entire en face and cross-sectional OCT image series were used, which covered a ~10 mm × 16 mm area. The en face OCT image series included images from all depths and readers were trained to recognize structural variations of mucosal patterns vs. vascular structures at different depths.

The following workflow was used in the readings:

1. First, only en face viewing was enabled. Readers read the en face OCT image series at various depths and assessed en face OCT features. If a region with irregular mucosal patterns was identified, it was demarcated on the image. The confidence of the assessment was noted as "high" or "low."

2. Next, cross-sectional and en face viewing were enabled. Readers read the cross-sectional OCT image series at different longitudinal positions. The confidence of each assessment was noted as "high" or "low." If >5 atypical glands were identified, atypical glands were defined to be present and the frame number (longitudinal position) with most atypical glands was recorded.

3. After performing steps 1 and 2 sequentially on each dataset, the readers reviewed the “low confidence” datasets using both en face and cross-sectional views. The readers could then change his/her assessments and/or confidence of the assessments.

Appendix e5 Statistical analysis

All statistical calculations were performed in MATLAB (Mathworks, MA). Quantitative metrics were represented as mean (SD). Interobserver agreement was assessed using unweighted kappa statistics, where <0.21 was defined as poor, 0.21 to 0.4 was fair, 0.41 to 0.6 was moderate, and 0.61 to 0.8 was substantial agreement. The *t* test was used to compare reading times of en face and cross-sectional OCT features. The Cochran–Mantel–Haenszel test was used to assess the association between OCT features and correlated histological diagnosis and treatment history stratified across different readers. A *P* value of <0.05 was considered statistically significant for all statistical tests in the manuscript.

Appendix e6 Supplemental discussion of differences between NBI and en face OCT

The en face OCT assessment used in this study was analogous to the recent NBI classification system (BING criteria), which showed 80% sensitivity and 88% specificity for identifying dysplasia by expert readers in a study of 97 patients [9]. Despite the similarity to NBI, en face OCT has a distinct appearance because OCT has different contrast mechanisms and resolution. NBI uses visible light to illuminate tissue and therefore visualizes predominantly superficial features. The reflected/scattered light is collected without depth information. OCT uses infrared light, which has deeper tissue penetration and detects depth-resolved differences in light backscattering from mucosal architecture [10]. OCT visualizes subsurface features, but the appearance of deeper structures are affected by optical attenuation and scattering from superficial structures. Subsurface en face OCT can mitigate deleterious effects of surface reflections and debris on image quality and has improved contrast/resolution compared with NBI. En face and cross-sectional views are intrinsically co-registered and specific features in en face OCT images can be viewed simultaneously in registered cross-sectional images or vice versa. Finally, OCT does not require contrast agents and can be used after biopsy/EMR [11], where visibility with NBI can be reduced by bleeding.

Appendix e7 Supplemental discussion of features in NDBE datasets

Features associated with neoplasia were also observed in NDBE datasets at higher than expected rates. En face OCT irregular mucosal patterns were observed in 35% of the NDBE datasets, suggesting that if this feature was used to detect neoplasia it would have a moderate specificity. This specificity is lower than recent NBI studies that use analogous criteria to assess mucosal patterns [9]. Possible reasons for these results include the following.

1. Sampling error – the majority of irregular mucosal patterns in en face OCT in NDBE were focal regions within regular mucosal patterns. As discussed in the Methods, OCT datasets were categorized as NDBE and included only if they were from patients without a history of dysplasia and with correlated histology of NDBE. Biopsy/EMR under OCT guidance was not performed in our study and was not approved by our Institutional Review Board. Biopsies from NDBE patients were taken following Seattle protocol and thus there was a possibility of sampling error. OCT datasets covered a >10 times larger area than sampled by standard pinch biopsy forceps and focal dysplastic regions may be missed by biopsy. However, it is unlikely that sampling error could explain a 35% rate of irregular mucosal patterns in NDBE. Future studies using laser marking techniques can allow more precise histological correlation with OCT images [12].

2. Previous studies showed that the OCT catheter can compress tissues and alter the mucosal architecture in cross-sectional images [13,14]. In this study we also noticed that excessive catheter pressure on tissue distorted mucosal patterns in en face OCT images. **Fig. e6** shows this effect in two NDBE datasets acquired with varying catheter pressure. With increasing catheter pressure, mucosal layer thickness decreased and regular mucosal patterns appeared distorted. Although it is challenging

to control the pressure exerted by the catheter, it is possible to re-acquire datasets with pressure artifacts, such as in **Fig. e6b**. However, this is limited by endoscopy time constraints. It is likely that similar pressure artifacts occur with VLE imaging balloons.

Atypical glands were also present at unexpectedly high rates, in 59% of the NDBE datasets (**Table e5**). To investigate, we stratified the NDBE data according to BE segment length and longitudinal imaging location with respect to the gastroesophageal junction (GEJ) (**Table e5**). Atypical glands were present in 78% of the NDBE datasets from short-segment (≤3 cm) NDBE patients vs. 43% of the NDBE datasets from long-segment (>3 cm) NDBE patients ($P < 0.001$). Furthermore, in the long-segment cohort, 67% of atypical glands were found ≤3 cm from the GEJ vs. 28% >3 cm from the GEJ ($P = 0.003$). The NDBE OCT datasets were obtained at standardized positions relative to the GEJ and covered a larger area than sampled by standard pinch biopsy, so it is difficult to biopsy glands. There is a high density of non-neoplastic cardiac glands in the cardia and near the GEJ, which could be misinterpreted as atypical glands [15,16] (see discussion in main text). Further studies with higher resolution OCT and more precise histological correlation are needed to assess whether OCT can detect differences between cardiac vs. atypical glands near the GEJ.

Appendix e8 Association of en face OCT with cross-sectional OCT

The association of mucosal patterns on en face OCT with individual cross-sectional OCT features was also assessed by stratifying according to correlated histological diagnosis, treatment history, and BE length **(Table 7, Table e10**). Atypical glands were present under irregular mucosal patterns in 44% of datasets (NDBE and neoplasia) vs. under regular mucosal patterns in 20% of the datasets (NDBE and neoplasia, $P < 0.001$), suggesting a general association of atypical glands with irregular mucosal patterns. However, there was poor association of absent mucosal layering and surface signal>subsurface with irregular mucosal patterns ($P = 0.7$ and $P = 0.76$, respectively) (**Table e10**).

Appendix e9 Supplemental discussion on association of en face OCT and VLE-DA criteria

The association of en face OCT irregular mucosal patterns and cross-sectional VLE-DA criteria with correlated histological diagnosis and treatment history are shown in **Table e11**. En face OCT irregular mucosal patterns and VLE-DA criteria for dysplasia were present in 23% of NDBE datasets vs. 77% of neoplasia datasets ($P < 0.001$) and in 92% of treatment-naïve neoplasia datasets.

Appendix e10 Supplemental discussion of high-confidence readings

Given limited sample size and variability in reader OCT experience, we asked readers to rate their confidence for each feature assessment in order to assess robustness of feature recognition and estimate potential performance improvement with additional training/experience, as in previous NBI and CLE studies [9,17]. In 81% of datasets, all features were assessed with high confidence (**Table e12**), suggesting that even readers with limited OCT experience can make assessments after brief training (average training time of 77 minutes).

Acknowledgment

We acknowledge Mehmet E. Ahsen at the Icahn School of Medicine at Mount Sinai for his assistance in the statistical analysis.

Supplementary References

1 Tsai TH, Ahsen OO, Lee HC et al. Endoscopic optical coherence angiography enables 3-dimensional visualization of subsurface microvasculature. Gastroenterology 2014; 147: 1219–1221

2 Wolfsen HC, Sharma P, Wallace MB et al. Safety and feasibility of volumetric laser endomicroscopy in patients with Barrett's esophagus (with videos). Gastrointest Endosc 2015; 82: 631–640

3 Ahsen OO, Lee HC, Giacomelli MG et al. Correction of rotational distortion for catheter-based en face OCT and OCT angiography. Opt Lett 2014; 39: 5973–5976

4 Phoa KN, van Vilsteren FG, Weusten BL et al. Radiofrequency ablation vs endoscopic surveillance for patients with Barrett esophagus and low-grade dysplasia: a randomized clinical trial. JAMA 2014; 311: 1209–1217

5 Leggett CL, Gorospe EC, Chan DK et al. Comparative diagnostic performance of volumetric laser endomicroscopy and confocal laser endomicroscopy in the detection of dysplasia associated with Barrett's esophagus. Gastrointest Endosc 2016; 83: 880–888 e882

6 Swager AF, Tearney GJ, Leggett CL et al. Identification of volumetric laser endomicroscopy features predictive for early neoplasia in Barrett's esophagus using high-quality histological correlation. Gastrointest Endosc 2017; 85: 918–926 e917

7 Evans JA, Poneros JM, Bouma BE et al. Optical coherence tomography to identify intramucosal carcinoma and high-grade dysplasia in Barrett's esophagus. Clin Gastroenterol Hepatol 2006; 4: 38–43

8 Kikinis R, Pieper SD, Vosburgh KG. 3D Slicer: a platform for subject-specific image analysis, visualization, and clinical support. In: Jolesz FA, ed. Intraoperative imaging and image-guided therapy: New York: Springer; 2014: 277–289

9 Sharma P, Bergman JJ, Goda K et al. Development and validation of a classification system to identify high-grade dysplasia and esophageal adenocarcinoma in Barrett's esophagus using narrow-band imaging. Gastroenterology 2016; 150: 591–598

10 Liang K, Ahsen OO, Lee HC et al. Volumetric mapping of Barrett's esophagus and dysplasia with en face optical coherence tomography tethered capsule. Am J Gastroenterol 2016; 111: 1664–1666

11 Ahsen OO, Lee HC, Liang K et al. Ultrahigh-speed endoscopic optical coherence tomography and angiography enables delineation of lateral margins of endoscopic mucosal resection: a case report. Therap Adv Gastroenterol 2017; 10: 931–936

12 Swager AF, de Groof AJ, Meijer SL et al. Feasibility of laser marking in Barrett's esophagus with volumetric laser endomicroscopy: first-in-man pilot study. Gastrointest Endosc 2017; 86: 464–472

13 Sivak MV, Jr., Kobayashi K, Izatt JA et al. High-resolution endoscopic imaging of the GI tract using optical coherence tomography. Gastrointest Endosc 2000; 51: 474–479

14 Westphal V, Rollins AM, Willis J et al. Correlation of endoscopic optical coherence tomography with histology in the lower-GI tract. Gastrointest Endosc 2005; 61: 537–546

15 Nakanishi Y, Saka M, Eguchi T et al. Distribution and significance of the oesophageal and gastric cardiac mucosae: a study of 131 operation specimens. Histopathology 2007; 51: 515–519

16 Huang Q. Controversies of cardiac glands in the proximal stomach: a critical review. J Gastroenterol Hepatol 2011; 26: 450–455

17 Kuiper T, van den Broek FJ, van Eeden S et al. Feasibility and accuracy of confocal endomicroscopy in comparison with narrow-band imaging and chromoendoscopy for the differentiation of colorectal lesions. Am J Gastroenterol 2012; 107: 543–550

18 Yao K. Zoom gastroscopy: magnifying endoscopy in the stomach: Springer Japan; 2013

19 Canto MI. Endomicroscopy of Barrett's esophagus. Gastroenterol Clin North Am 2010; 39: 759–769